Acoustic impedance and interface phonon scattering in Bi₂Te₃ and other semiconducting materials

Xin Chen, David Parker, and David J. Singh

Oak Ridge National Laboratory, 1 Bethel Valley Road, Oak Ridge, Tennessee 37831, USA
(Received 6 September 2012; revised manuscript received 11 December 2012; published 30 January 2013)

We present first-principles calculations of the phonon dispersions of Bi₂Te₃ along with calculations of the sound speed anisotropy for a number of materials, and we discuss these in relation to acoustic phonon interface scattering in ceramics. The Bi₂Te₃ phonon dispersions show agreement with what is known from neutron scattering for the optic modes, while we find a difference between the generalized gradient approximation and local density results for the acoustic branches. This is a consequence of an artificial compression of the van der Waals bonded gaps in the Bi₂Te₃ structure when using the generalized gradient approximation. As a result, local density approximation calculations provide a better description of the phonon dispersions in Bi₂Te₃. A key characteristic of the acoustic dispersions in several materials studied is the existence of a strong anisotropy in the velocities. Such an anisotropy may be a significant consideration in the reduction of lattice thermal conductivity by nanograin boundary scattering. This is a well-known technique commonly employed to improve thermoelectric performance. We develop a model to quantify the effect of this anisotropy for this interface scattering in ceramics, and we apply this to Bi₂Te₃ and compare with PbTe and several other semiconductors.

I. INTRODUCTION

Thermoelectric performance is commonly quantified in terms of a dimensionless parameter ZT, defined as follows:

$$ZT = \frac{S^2 \sigma T}{\kappa}. \qquad (1)$$

Here S is the Seebeck coefficient, σ is the electrical conductivity, and κ is the thermal conductivity. It is usually a good approximation to treat κ as being comprised of a lattice portion and an electronic portion. The electronic portion is directly related to the electrical conductivity by the Wiedemann-Franz relation (usually a good approximation for the heavily doped semiconductors that are useful thermoelectrics), leading to the point that, from a standpoint of materials optimization, the lattice thermal conductivity represents wasted heat transfer and should be as small as possible. One realization of this is the "phonon glass electronic crystal" (PGEC) concept of Slack,[1] in which phonons are strongly scattered, leading to low lattice thermal conductivity, while the charge carriers are not strongly scattered. The filled skutterudites[2–4] represent an apparent realization of the PGEC concept. Another approach toward the PGEC concept is the use of nanostructuring from compaction and sintering of a nanosize powder into a ceramic. The mean free path for phonons in bulk crystalline thermoelectrics is often one to two orders of magnitude larger than that for electrons, so the use of grain sizes in between these two mean free paths will tend to strongly scatter phonons, but not electrons. This approach has been successfully applied to Bi₂Te₃,[5,6] raising the ZT values near room temperature from the previously found value of 1.0 to an impressive 1.5. A similar scenario could also apply to hole-doped Bi₂Se₃.[7] Note that there are various types of grain boundary scattering that can reduce the thermal conductivity, such as insulating interstitial material, but typically these destroy the electrical conductivity, preventing good thermoelectric performance. In this respect, the sintering of polycrystalline samples (as opposed to simply compressed powder) is important as it assures good electrical contact between the nanograins while maintaining interface

scattering. Understanding interface phonon scattering at such electrically conducting interfaces is therefore of importance.

One factor as yet unaddressed, however, is the role of phononic anisotropy in producing phononic scattering. Consider by analogy, for example, the case of light propagation in dense ceramics. In that case it is known that fine-grained ceramics of optically isotropic materials can be made transparent,[8] while this is not the case for anisotropic materials with random grain orientation. In the former case, despite the small grain sizes, light is able to pass through the material because there is not significant scattering at the grain boundaries. The reason for this is that the light speed does not change at the grain boundary, so there is no impedance (or velocity) mismatch. While the acoustic case differs from the optical case due to the presence of the longitudinal mode, the velocity mismatch still applies.

We note also that, unlike in optics where there is no optical anisotropy in cubic materials, a cubic material can have a rather anisotropic elastic response tensor (the tensor of elasticity C_{ijkl}) and hence sound speed—a good example of such a material is PbTe, as described in more detail in the final section. This material shows comparable anisotropy to Bi₂Te₃ despite being cubic. The reason for this is that the response tensor for optics—the dielectric constant tensor—is a *second*-rank tensor whose off-diagonal elements must necessarily vanish due to the cubic symmetry. However, no such restriction applies to the *fourth*-rank tensor of elasticity, and indeed the sound velocity in a cubic material can vary significantly by direction, as will be evident for PbTe.

Note that for heat transport in crystalline solids, it is the longer wavelength acoustic modes that dominate heat transport due to the presence of a significant group velocity—the sound speed. The main point of this paper is that it is this sound velocity mismatch that is ultimately responsible for the efficacy of grain boundary scattering, and that this mismatch can be quantitatively assessed by considering the sound velocity anisotropy. We are working here in the limit in which the phonon mean free path is larger than the nanograin size, so

that transport within a grain is in the ballistic limit, as was considered in a different context in Ref. 9. In this limit, the lattice thermal conductivity will be predominated by the size of the nanograins and not the diffusive scattering, as was considered in Ref. 10.

We provide a definition, and examples of, simple dimensionless parameters R and S, easily computable if the elastic constants are known, that should provide valuable information about the ability of nanostructuring (of a type that yields grains in intimate contact) to reduce lattice thermal conductivity. We will make direct application of our findings to Bi_2Te_3, which, as already mentioned, has already shown substantial performance benefits from nanostructuring, and in addition PbTe and several other semiconductors. One conclusion to be drawn from our work is that, unlike in electronic transport where anisotropy can be destructive to thermoelectric performance, anisotropy is generally beneficial in phononic transport because it enhances the effects of nanostructuring in reducing the lattice thermal conductivity.

II. PHONON AND ELASTIC CONSTANT CALCULATIONS FOR Bi_2Te_3

With an eye toward the effects of nanostructuring in reducing $\kappa_{lattice}$ and enhancing ultimate performance, we have computed the phonon dispersions and density of states for Bi_2Te_3, the best known and most studied thermoelectric. Our calculations are based upon density functional theory in the framework of Blöchl's projector augmented-wave (PAW) method[11] within the local density approximation (LDA) as implemented in VASP.[12] We also did generalized gradient approximation calculations but found that they are not as accurate as the LDA results (see below). A $3 \times 3 \times 3$ k-point grid in a $3 \times 3 \times 3$ supercell was used, along with an energy cutoff of 300 eV. Cell parameters and internal coordinates were both relaxed until internal forces were less than 2 meV/Å. From the computed electronic structure, one performs several supercell calculations incorporating "frozen-phonons," or atomic displacements dictated by the rhombohedral crystal symmetry. By evaluating the forces on the displaced atoms, one may generate a basis set of force constants from which the phonon band structure and density of states are generated. We depict these in Fig. 1. Previous Bi_2Te_3 lattice-dynamics calculations were performed in Refs. 13–16. Spin-orbit coupling was not included and we therefore cannot assess the claim of Ref. 15 for evidence of a spin-orbit coupling-related lattice instability. Experimentally the material is known to be stable. Our calculations generally reproduce the non-spin-orbit coupling phonon dispersions of these authors.

One notes upon examination of the central region (the portions Z-Γ and Γ-L) that the three acoustic modes differ significantly in these two directions (c axis and in-plane, respectively). In particular, the highest velocity acoustic mode, the longitudinal acoustic, has significantly lower velocity in the c-axis direction Γ-Z than the nearly planar direction Γ-L; quantitatively, the c-axis longitudinal velocity is 1811 m/s and
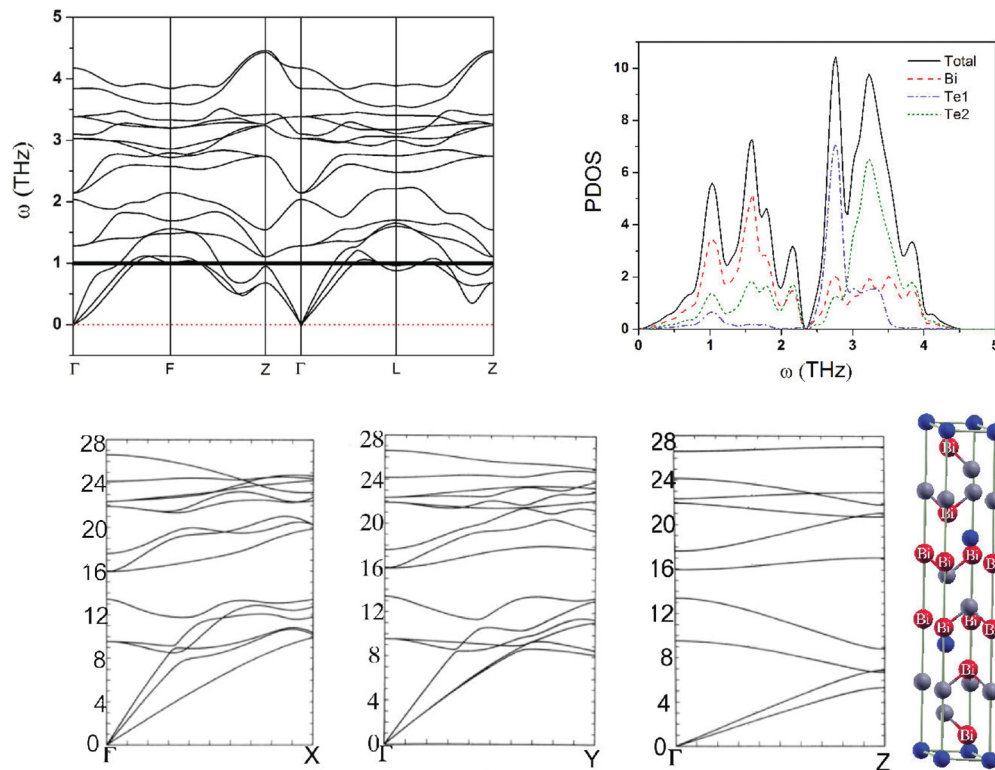

FIG. 1. (Color online) The computed phonon dispersions (top left) and associated density of states (top right) of Bi_2Te_3. Coordinate momenta (units of reciprocal rhombohedral lattice vector): L: (1/2,0,0); F: (1/2,0,1/2); Z: (1/2,1/2,1/2). The heavy black line in the left figure indicates the upper frequency limit of the predominant heat carrying acoustic modes. Bottom: the measured phonon dispersions, in 10^{12} rad/sec, from Ref. 20 and a picture of the physical structure of Bi_2Te_3. Phonon dispersions from left: Γ-X, Γ-Y, Γ-Z. In the structure picture, Te1 is in blue (located at top and bottom) and Te2 in gray (second layer from the top and bottom).

the planar is 2394 m/s, a difference of about 30%. In addition, the transverse acoustic modes are degenerate from Γ-Z but not so in-plane; here the velocities are significantly different as well, with the single c-axis value of 1774 m/s and the two planar velocities of 1395 and 1728 m/s. These velocities are low and generally typical of good thermoelectric materials. Note also that in the frequency range at and above 1 THz, the optic modes intersect with the acoustic modes, so that the primary region of heat transport is limited to less than 1 THz, which in turn limits the phonon momenta that contribute to transport to locations relatively near the Γ point.

Turning to the phonon density of states, one finds three regions of interest. Highest in frequency, as expected given the lighter mass, are the primarily Te optic modes between 2.3 and 4 THz. As noted previously, these modes are not the primary contributors to phononic transport due to the very small group velocities (see the left-hand panel of Fig. 1), although they do make some contribution. A similar statement applies to the primarily Bi optic modes between 1 and 2.3 THz, although these may be important contributors to phononic scattering due to anharmonic scattering of the lower-frequency acoustic modes, which are at frequencies less than 1.5 THz. As noted above, only a fraction of these modes—those less than 1 THz— contribute to thermal transport as the higher-frequency acoustic modes are strongly scattered by the adjacent optic modes, and also have smaller group velocities. For example, in the Γ-L direction, only those acoustic phonons less than half the L-point momentum will strongly contribute to heat transport, while in the Γ-F direction this cutoff frequency occurs at a momentum roughly 60% of the F-point momentum. It should be noted that the later discussion of sound speed anisotropy as a contributor to nanograin scattering is an approximation which effectively assumes that *all* phononic transport derives from the acoustic modes, which is clearly somewhat simplified compared to reality, as the optic modes in Fig. 1 do in fact exhibit some dispersion and hence heat transport. Nevertheless, it is likely that the majority of transport indeed derives from the acoustic modes.

The original lattice-dynamics calculations for this work employed the standard GGA.[17,18] However, these results produced longitudinal sound speed velocities which were higher in the Γ-Z direction (the c axis) than in the planar directions. This result persisted even when a relatively fine $4 \times 4 \times 4$ k-point mesh was used. Similarly, we initially found from first-principles calculations of the elastic constants of Bi_2Te_3 using WIEN2K (Ref. 19) and the GGA that the elastic constants c_{11} and c_{33} are very nearly equal. All these results are contrary to the elastic constant data of Jenkins,[20] which produce higher longitudinal sound speeds in-plane (see the next section), as well as the measured planar and c-axis thermal conductivity,[21] where the c-axis value is less than half the planar value, indicating lower c-axis sound speeds. Our calculational discrepancy was likely due to the common GGA overestimation of lattice constants. It was for this reason that we performed these lattice-dynamics calculations within the LDA, which often gives structural and elastic properties in better agreement with experiment.[22,23] These results suggest that for anisotropic layered semiconductors such as Bi_2Te_3, use of the LDA to compute elastic and lattice dynamics properties may be desirable.

TABLE I. Calculated elastic constants (in GPa) for Bi_2Te_3.

Approximation	c_{11}	c_{12}	c_{13}	c_{33}
LDA	83.8	3.8	32.1	54.5
GGA	97.4	21.4		90.4

For a direct comparison with experiment, included in Fig. 1 are plots of the phonon dispersions deduced by Jenkins. While exact in-plane comparisons are not possible due to Jenkins' choice of Γ-X and Γ-Y dispersion directions, we note that as in our calculated results, the Γ-Z sound speed is lower than the planar values. In general, there is a reasonable correspondence between Jenkins' results and ours, with the Γ-Z acoustic modes reaching values of ~ 0.8–1 THz in both cases (note that Jenkins' data are presented in rad/s whereas ours are in Hz). At the Z point, Jenkins' optic mode frequencies are 7, 9, 17, 21, 23, and 27×10^{12} rad/s, which compare rather well with our values of 1.2, 1.6, 2.7, 3.3, 3.5, and 4.5 THz. At the Γ point, Jenkins' optic mode frequencies are approximately 9.5, 13.5, 16, 17.7, 22, 22.5, 24, and 26.5×10^{12} rad/s, which again compare well with our values (in 10^{12} Hz) of 1.3, 2, 2.2, 3, 3.1, 3.4, 3.8, and 4.2. The experimental sound speeds from Γ-Z are also approximately equal to our calculated values, from a comparison of the figures. All in all, the good agreement suggests the accuracy and applicability of our lattice dynamics calculations on Bi_2Te_3.

For the lattice-dynamics calculations, LDA-optimized internal coordinates and lattice parameters (4.35 Å planar, 29.82 Å c axis) were used, while for the elastic constant calculations experimental lattice parameters of 4.386 Å planar and 30.50 Å c axis (but LDA-optimized internal coordinates) were employed. As is well known, van der Waals interactions can be important for layered materials such as Bi_2Te_3, and while these are not included in our functionals, we do find good agreement with the experimental properties in the lattice-dynamics calculations, as indicated. The elastic constant calculations (see Table I) exhibit somewhat larger discrepancies with experiment (see Table III), even with usage of the LDA, with (for example), the value of c_{12} calculated as 3.8 GPa, much smaller than the experimental value of 22.0 GPa. We ascribe this to the difficulty of incorporating all bonding effects in layered materials such as Bi_2Te_3 into the simple LDA. For these calculations, we used between 182 and 770 k points in the irreducible portion of the Brillouin zone (note that the elastically distorted Brillouin zone need not retain the hexagonal symmetry), and we employed spin-orbit coupling except for the optimizations and LAPW sphere radii of 2.5 Bohr radii.

Since above we describe the effect of using the LDA for *structural* properties of layered semiconductors such as Bi_2Te_3, it is worthwhile to ask about the effect of using the LDA for *electronic* properties of Bi_2Te_3. Therefore, in Fig. 2 we present the calculated electronic structure of Bi_2Te_3 within both the GGA *and* LDA approximations (calculated using WIEN2K) where all other relevant quantities such as LAPW sphere radii (2.5 Bohr radii for all atoms), k points (2000 in the full Brillouin zone), and lattice parameters (4.386 Å planar and 30.50 Å c axis) and atomic coordinates are assumed identical. We have used spin-orbit coupling for
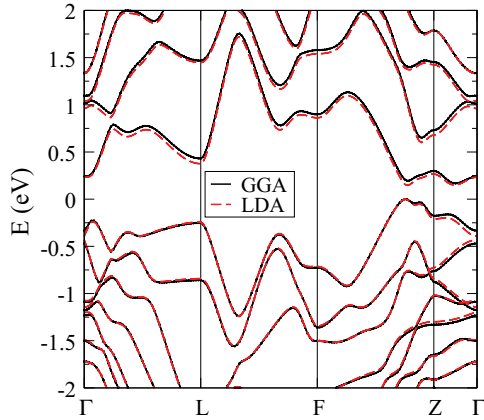
FIG. 2. (Color online) The computed band structure of Bi_2Te_3 within the LDA and GGA approximations. Note the relatively small differences in the band structures.

these calculations as this generally affects electronic structure much more substantially than structural properties. As the plot indicates, there is only a very small difference between the two electronic structures, mainly concerning the exact value of the gap at the conduction-band minimum.

III. SOUND SPEED ANISOTROPY AND NANOSTRUCTURING EFFECTIVENESS PARAMETERS

The discussion of the preceding section makes plain the significant anisotropy in the phonon transport of Bi_2Te_3. Here we find a way to assess the quantitative impact of this anisotropy in reducing lattice thermal conductivity, and we make a comparison with another well-studied thermoelectric material, PbTe, as well as diamond and several other semiconductors.

In this discussion, we will implicitly assume that the grain boundary scattering is in the ballistic regime, which will be obtained when the average phonon mean free path (that would occur in the absence of grain boundaries) becomes comparable to or larger than the grain size. More specifically,

we will assume that at least a significant fraction of the distribution of these phonon mean free paths is larger than the nanograin size, so that there is significant ballistic scattering at the grain boundaries. In this limit, the well-established acoustic mismatch theory[24–27] describing heat conduction at interfaces of crystalline solids can be applied, as is described below.

Our method is the following. From published calculated values of the elastic constants for Bi_2Te_3, one may generate the associated Christoffel[28] elastic tensor stiffnesses and solve the resulting secular equation for the three sound velocities (one longitudinal and two transverse) as a function of the wave propagation direction. The relevant equations may be found in Ref. [29] and are summarized in the Appendix. We have plotted up the sound speeds, as a function of propagation direction, in Fig. 3. The sound speed plots differ significantly from a spherical shape, underscoring the anisotropy already apparent from the calculated phonon band structure.

We turn now to the impact of the anisotropic sound speeds on the lattice thermal conductivity. As is well known, the lattice thermal conductivity κ_l is given as

$$\kappa_l = \sum_{\mathbf{q},i} C_{\mathbf{q},i} v_{\mathbf{q},i} \ell_{\mathbf{q},i}, \tag{2}$$

where $C_{\mathbf{q},i}$ is the specific heat attributable to a phononic mode with momentum $\mathbf{q}$ and polarization i, v is the sound speed of that mode, ℓ is the mean free path of that mode, and a sum over the modes of significant group velocity is taken. In general, the fraction R of elastic energy reflected at a grain boundary interface at normal incidence is given by the impedance mismatch formula:

$$R = \left(\frac{(Z_1 - Z_2)}{(Z_1 + Z_2)} \right)^2. \tag{3}$$

Here Z_1 and Z_2 are the acoustic impedances of the two adjoining grains, given by $Z_i = \rho_i v_i$, where ρ is the density of a grain and v is the sound speed (of a given polarization) within the grain. Since we expect ρ to be constant within a nanostructured sample, the energy fraction reflected depends on the sound speeds v_1 and v_2 in the two grains, *at the*
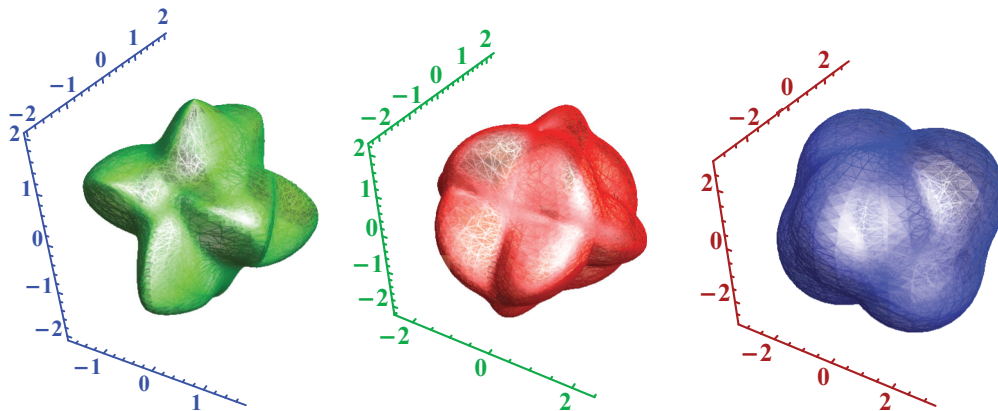

FIG. 3. (Color online) The computed sound speed anisotropy of Bi_2Te_3. Distance from origin represents sound speed, in km/s, for that direction of propagation. Transverse modes $T1$ and $T2$, left and center, respectively; longitudinal mode, right. Elastic constants taken from Ref. [20].
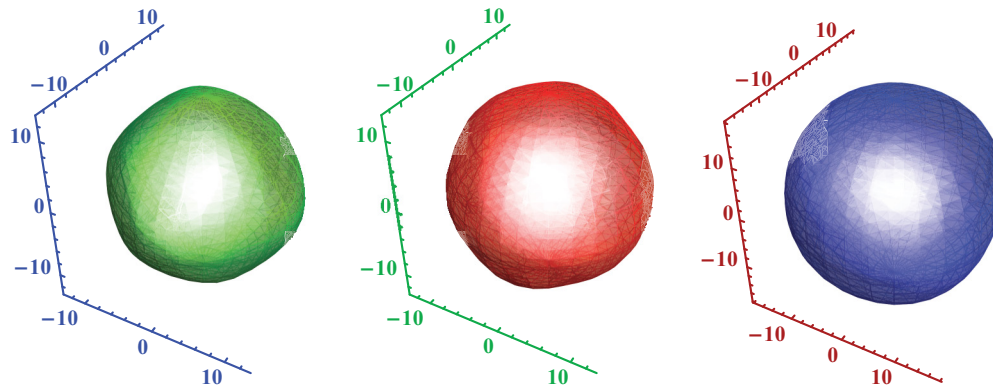
FIG. 4. (Color online) The computed sound speed anisotropy of diamond. Elastic constants taken from Ref. 34. Transverse modes, left and center; longitudinal mode, right.

directions of incidence and transmission, and in addition on the polarization of the incoming wave. Note also[30] that an incident wave of one polarization may induce scattered waves of other polarizations, complicating the issue further. Furthermore, in a nanostructured sample we do not expect oriented grains. Hence to work out the effective grain boundary scattering rate, one must consider grain orientation as well as the intrinsic anisotropy of the sound speeds. This becomes a rather difficult, and even difficult to formulate, problem when one realizes that the grains are not likely to be exactly randomly oriented, and that the degree of randomness will likely depend on the exact synthesis and nanostructuring techniques applied, unknown in this work.

Given that one purpose of this paper is to propose computationally simple nanostructuring effectiveness parameters, we therefore make a simple ansatz based upon the (relatively) random nature of the problem at hand. Since the incident and transmitted velocities v_1 and v_2 are essentially uncorrelated, it is a fair approximation to replace v_2 in the above impedance mismatch expression by its average value (a similar assumption in a different context is made in many "mean-field" theories) and integrate over all angles of incidence. As with mean-field theories, the simpler expression is most quantitatively accurate when v_1 does not vary too much from its average. The gross features of anisotropy, however, should be reasonably well captured by this expression. The expression for R_{tot} is a simple two-dimensional integral:

$$R_{tot} = \frac{1}{4\pi} \int \sin(\theta) d\theta \, d\phi \left(\frac{v(\theta,\phi) - v_{av}}{v(\theta,\phi) + v_{av}} \right)^2, \quad (4)$$

where the above integral is computed for each of the two transverse modes and the longitudinal mode and then averaged over the modes. One could argue, based on phase-space considerations, that the various terms should be weighted by the sound speeds, or sound speeds squared, or some other factor, of the various modes, but it is usually unclear in any given system what fraction of heat transport separately results from transverse and longitudinal modes,[31] so we have retained the simplest possible expression.

The above expression yields a single number R_{tot}, which gives in essence the average impedance mismatch reflected energy *at normal incidence* for a single scattering event. It is typically fairly small—of the order of 0.01 or less even

for highly anisotropic media, as depicted below. However, there is an important additional scattering effect created by the velocity anisotropy. As with propagation of electromagnetic waves, there is a form of Snell's law, $v_{incoming}/v_{transmitted} = \sin(\theta_{incoming})/\sin(\theta_{transmitted})$, relating incoming and outgoing propagation angles (relative to the normal) to the relative sound speeds, and a version of total internal reflection, in which for certain angles of incidence there is *no* energy transmission across the interface, applies. To put this quantitatively, for a 20% smaller sound speed (in a given direction) in the receiving material, angles of incidence greater than 53°—40% of the possible angles of incidence—result in total internal reflection, even though the impedance mismatch reflection coefficient at normal incidence is only 0.012. This point is described well quantitatively in the reference of Little.[9] Since the *average* sound speeds in the two nanograins are of course equal, what one needs is a measure of the average deviation of the velocity from its average, which in essence is what the individual R_i measures (more precisely speaking, $R_i \simeq \frac{(\Delta v_i)^2}{4v_{i,av}^2}$, where Δv is the standard deviation of v_i and $v_{av,i}$ is the angular average sound velocity of a mode of polarization i).

To give examples of velocity anisotropy and R_{tot}, we have computed and present in Figs. 3–5 the sound speed anisotropy for three well-known semiconducting materials: Bi_2Te_3, diamond, and PbTe, respectively. Diamond is included to demonstrate a material with very low elastic anisotropy, while PbTe and $CoSb_3$ are well known thermoelectrics. We will see that as expected, Bi_2Te_3 shows significant potential for nanostructuring reductions of $\kappa_{lattice}$. As mentioned previously, despite its cubic structure, PbTe also shows large velocity anisotropy. As asserted previously, while its cubic nature ensures isotropic conductivity, there is no such requirement on the elastic properties. Its elastic anisotropy might therefore also be expected to allow good reductions of lattice thermal conductivity due to nanostructuring, but recent work[32] shows that for PbTe these nanostructures must be smaller than 10 nm to have a significant effect, as the phonon mean free path is already very short. Conversely, although diamond shows very low anisotropy, its phonon mean free path is so long (well over 100 nm) that small-grain nanostructuring would likely have a significant impact on its lattice thermal conductivity (noting nevertheless the impracticality of this material for thermoelectric applications). We have taken account of this
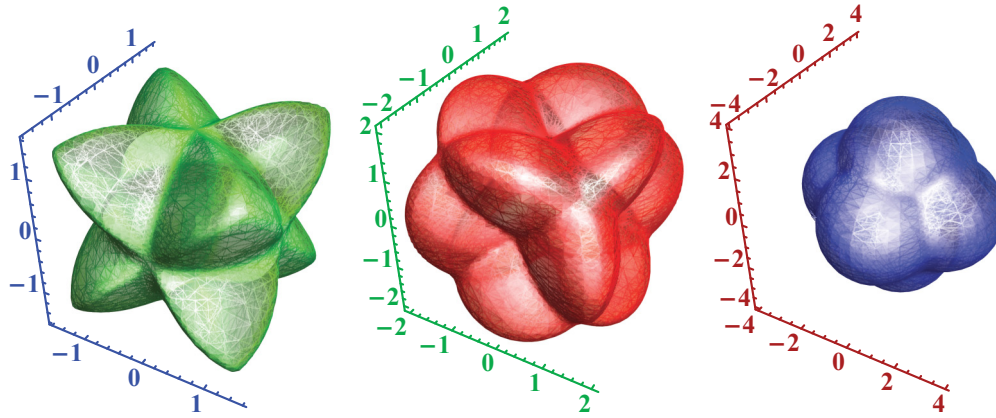
FIG. 5. (Color online) The computed sound speed anisotropy of PbTe. Elastic constants taken from Ref. 35. Transverse modes, left and center; longitudinal mode, right.

additional effect by defining a "scattering potential coefficient" S_{tot} as $R_{tot}\kappa_{lattice,bulk}/\kappa_{min}$, where $\kappa_{lattice,bulk}$ is self-explanatory (values for Bi_2Te_3 and PbTe taken from Ref. 21) and κ_{min} is the "minimum thermal conductivity,"[33] which we simply take as 0.5 W/m K for all materials studied.

In an attempt to quantify the anisotropy presented in Figs. 3–5, in Table II we present the average impedance mismatch scattering reflection coefficient R for each of the three materials, along with $CoSb_3$, GaAs, and Si. As expected, diamond has by far the lowest impedance reflection coefficient, with an average R between one and two orders of magnitude less than PbTe and Bi_2Te_3. The large values for PbTe suggest that, as with Bi_2Te_3, nanostructuring may yet be effective in reducing $\kappa_{lattice}$ if sufficiently small nanograins can be formed. With regard to $CoSb_3$, note that while this material shows significant potential for nanostructuring lattice thermal conductivity reduction (since S_{tot} is substantial), this reduction would be proportionately smaller for a high-performance skutterudite such as a triple-filled material, since the lattice term has already been reduced substantially by the "rattling" effect. Hence high-performance skutterudites would be expected to show smaller performance benefits from nanostructuring than PbTe and Bi_2Te_3. Conversely, as observed in Ref. 37, substantial $\kappa_{lattice}$ reductions—as much as 80%—occur in nanostructured $CoSb_3$ without added "rattlers." The very small values of R for diamond provide a natural explanation for why polycrystalline diamond is such a good heat conductor. We have not included the thermoelectric half-Heusler compounds due to a paucity of data and a great variability[38–42] in anisotropy

in the few data that do exist. For Bi_2Te_3, the lattice thermal conductivity given is the planar value; the c-axis value is roughly half this.

IV. DISCUSSION AND PROPOSED EXPERIMENTAL TEST OF THEORY

The results of the preceding section attempt to define a nanostructuring "figure-of-merit," and the scattering potential coefficient S_{tot} which we hypothesize will correlate with the ability of nanostructuring to reduce lattice thermal conductivity. In the last two columns of Table III, we present the parameters S_{tot} and the measured reduction in thermal conductivity, relative to single-crystal values, of nanostructuring or, in the absence of such data, of polycrystalline samples. There is an obvious correlation between the two parameters, but it is not clearly better[49] than a simple correlation between the measured thermal conductivity reduction and the single-crystal thermal conductivity values; in particular, Bi_2Te_3 and $CoSb_3$ show very different $\kappa_{lattice}$ reductions despite nearly equal S_{tot} values. The reason for this, we believe, is simply that the grain sizes in the nanostructured (or for that matter, polycrystalline) samples are not the same from one material to another, so that this is not an "apples-to-apples" comparison.

To make such a comparison, let us consider the thermal conductivity of a nanostructured sample with two sources of scattering: the phonon-phonon scattering commonly dominating $\kappa_{lattice}$ for temperatures above the Debye temperature, and grain boundary scattering from the nanograins. One may then

TABLE II. Average impedance mismatch reflection coefficients (multiplied by 100), scattering potential coefficients, and experimental lattice thermal conductivity reductions for several materials. L refers to the longitudinal mode and $T1$ and $T2$ to the transverse modes. The skutterudite values in parentheses indicate typical values for a high-performance thermoelectric skutterudite.

Compound	R_L	R_{T1}	R_{T2}	R_{tot}	$\kappa_{lattice,bulk}$ (W/m K)	S_{tot}	$\kappa_{lattice}$ reduction from nano/polycrystalline
Bi_2Te_3	0.153	0.429	0.437	0.340	1.7 (planar)	1.16	1.4[6]
PbTe	0.187	0.544	0.850	0.527	2.3	2.42	
$CoSb_3$	0.0234	0.0623	0.133	0.0703	9 (3)	1.26 (0.42)	7[37]
diamond	0.006 27	0.0151	0.005 37	0.0089	2200	39.16	100[43]
GaAs	0.026 21	0.042 47	0.1436	0.0706	46[44]	6.51	38[45]
Si	0.016 68	0.1436	0.042 47	0.067 66	156[46]	21.11	142[47]

TABLE III. Elastic constants (in GPA) used in the calculation of sound speed anisotropies. All compounds except for Bi_2Te_3 are cubic and hence have only three independent elastic constants.

Compound	c_{11}	c_{12}	c_{33}	c_{44}	c_{13}	c_{14}
Bi_2Te_3	74.4	22.0	51.6	31.4	29.2	15.4
PbTe	128.1	4.4		15.1		
CoSb$_3$[36]	202.0	55.8		42.2		
diamond	1076	125		576		
GaAs[44]	118.4	53.7		59.1		
Si[48]	166	64.0		79.6		

write the total scattering rate, using Matthiesen's rule, as

$$\tau^{-1} = \alpha T + \beta v_s / d. \tag{5}$$

Here α and β are material-specific constants, d is the mean grain size, and v_s is a suitably averaged sound speed. β describes the efficacy of grain boundary scattering in a given material and α is the effectiveness of phonon-phonon scattering. The sound speed appears in this expression because higher sound speeds imply shorter times to traverse a nanograin and undergo a scattering event. Then one may write the thermal conductivity as

$$\kappa_{\text{lattice}} = \frac{C v_s^2}{\alpha\left(T + \frac{\beta v_s}{\alpha d}\right)}. \tag{6}$$

Here C is the specific heat, which we assume to be known. We may readily identify the quantity β/α with the scattering potential coefficient S_{tot}, since in our theory β expresses the relative effect of impedance mismatch scattering, and α is the effect of phonon-phonon scattering, which predominates κ_{lattice} in bulk materials.

To test this assertion, what is needed are two or more sets of thermal conductivity measurements on materials with rather different S_{tot} values, with each set comprising a series of tests of samples with nanograins of different sizes d. This would allow determination of the values of α/β for each of the two materials, which could then be compared with the calculated S_{tot} values. One caveat is that the above expression for the scattering time fails as one approaches the minimum thermal conductivity, so that measurements at lower temperatures (say 300 K) would likely be more accurate since κ is larger at low temperature.

This represents an attempt to isolate the effects of velocity anisotropy scattering from the numerous other factors affecting phononic transport in a real nanostructured sample, including (for example) the means of sample preparation and other microstructural properties. In addition, other forms of scattering, such as by soft interstitial material between grains, could be a significant contributor to reducing thermal transport. We do think, however, that the impedance and velocity mismatch associated with grain boundary scattering in nanostructured samples, as depicted here, can be a significant contributor to the reduction of thermal conductivity by nanostructuring, and that the quantitative parameters presented may give an indication of the likely effectiveness of nanostructuring in reducing the lattice thermal conductivity of a given material.

V. SUMMARY AND CONCLUSIONS

We present calculated phonon dispersions for Bi_2Te_3 and discuss ceramic grain boundary scattering in terms of acoustic impedance mismatch. We find that, as expected, grain boundaries may lead to strong interface scattering in Bi_2Te_3 nanostructured material. Interestingly, this is also expected to be the case in materials such as PbTe, which, although cubic, does have substantial acoustic wave anisotropy. This is in contrast to the optical case, where a cubic material would have no such scattering. In any case, the implication of the present results is that dense sintered ceramics of anisotropic material such as Bi_2Te_3 or PbTe will have reduced thermal conductivity provided that the appropriate grain size is used; we develop a method for quantifying this velocity anisotropy. In the case of more isotropic materials, other strategies for producing scattering at grain boundaries, such as the introduction of second phases (as studied in Refs. 50 and 51), may be needed.

APPENDIX

In this Appendix, we describe in somewhat more detail the method for extracting sound speeds from the elastic constants. For the sake of brevity, we will only demonstrate the most complex case depicted in the paper, i.e., that of rhombohedral Bi_2Te_3. In general, solving the Christoffel equations requires the solution of a 3×3 determinant equation, $\det[\Gamma - \lambda \mathbf{1}] = 0$. Here the eigenvalues λ are equal to $\rho v_{i,\theta,\phi}^2$, where ρ is the material density and $v_{i,\theta,\phi}$ is the sound speed of given polarization and propagation. The matrix Γ is the elastic stiffness matrix. For Bi_2Te_3 there are six nonzero elastic constants: c_{11}, c_{12}, c_{13}, c_{14}, c_{33}, and c_{44}. Then the components of the symmetric Γ matrix are given as follows[28] (here n_1, n_2, and n_3 are the direction cosines along the x, y, and z axes, which we take in spherical coordinates):

$$\Gamma_{11} = n_1^2 c_{11} + \frac{n_2^2}{2}(c_{11} - c_{12}) + n_3^2 c_{44} + 2 n_2 n_3 c_{14}, \tag{A1}$$

$$\Gamma_{22} = n_2^2 c_{22} + \frac{n_1^2}{2}(c_{11} - c_{12}) + n_3^2 c_{44} - 2 n_2 n_3 c_{14}, \tag{A2}$$

$$\Gamma_{33} = n_2^2 c_{44} + n_2^2 c_{44} + n_3^2 c_{33}, \tag{A3}$$

$$\Gamma_{23} = \Gamma_{32} = \left(n_1^2 - n_2^2\right) c_{14} + n_2 n_3 (c_{13} + c_{44}), \tag{A4}$$

$$\Gamma_{13} = \Gamma_{31} = n_1 n_3 (c_{13} + c_{44}) + 2 n_1 n_2 c_{14}, \tag{A5}$$

$$\Gamma_{23} = \Gamma_{32} = n_1 n_3 c_{14} + n_1 n_2 (c_{11} + c_{12})/2. \tag{A6}$$

Diagonalization of Γ then directly yields the eigenvalues λ and associated sound speeds $v_{i,\theta,\phi}$.

[1] G. A. Slack, in *CRC Handbook of Thermoelectrics*, edited by D. M. Rowe (CRC, Boca Raton, FL, 1995), pp. 407–440.

[2] B. C. Sales, D. Mandrus, and R. K. Williams, Science **272**, 1325 (1996).

[3] T. He, J. Chen, H. D. Rosenfeld, and M. A. Subramanian, Chem. Mat. **18**, 759 (2006).

[4] X. Shi, S. Bai, L. Xi, J. Yang, W. Zhang, L. Chen, and J. Yang, J. Mat. Res. **26**, 1745 (2011).

[5] B. Poudel, Q. Hao, Y. Ma, Y. Lan, A. Minnich, B. Yu, X. Yan, D. Wang, A. Muto, D. Vashaee, X. Chen, J. Liu, M. S. Dresselhaus, G. Chen, and Z. Ren, Science **320**, 634 (2008).

[6] W. Xie, X. Tang, Y. Yan, Q. Zhang, and T. M. Tritt, Appl. Phys. Lett. **94**, 102111 (2009).

[7] D. Parker and D. J. Singh, Phys. Rev. X **1**, 021005 (2011).

[8] H. Jiang, Y. K. Zou, Q. Chen, K. K. Li, R. Zhang, Y. Wang, H. Ming, and Z. Zheng, Proc. SPIE **5644**, 380 (2005).

[9] W. A. Little, Can. J. Phys. **37**, 334 (1959).

[10] E. T. Swartz and R. O. Pohl, Rev. Mod. Phys. **61**, 605 (1989).

[11] G. Kresse and D. Joubert, Phys. Rev. B **59**, 1758 (1999).

[12] Vienna Ab-initio Simulation Package, available from www.vasp.at.

[13] B. Qiu and X. Ruan, Phys. Rev. B **80**, 165203 (2009).

[14] B.-L. Huang and M. Kaviany, Phys. Rev. B **77**, 125209 (2008).

[15] B.-T. Wang and P. Zhang, Appl. Phys. Lett. **100**, 082109 (2012).

[16] W. Kullmann, G. Eichhorn, H. Rauh, R. Geick, G. Eckold, and U. Steigenburger, Phys. Status Solidi **162**, 125 (1990).

[17] J. P. Perdew, J. A. Chevary, S. H. Vosko, K. A. Jackson, M. R. Pederson, D. J. Singh, and C. Fiolhais, Phys. Rev. B **46**, 6671 (1992).

[18] J. P. Perdew and Y. Wang, Phys. Rev. B **45**, 13244 (1992).

[19] P. Blaha, K. Schwarz, G. K. H. Madsen, D. Kvasnicka, and J. Luitz, *WIEN2k, An Augmented Plane Wave + Local Orbitals Program for Calculating Crystal Properties* (Karlheinz Schwarz, Techn. Universitat Wien, Austria, 2001).

[20] J. O. Jenkins, J. A. Rayne, and R. W. Ure, Jr., Phys. Rev. B **5**, 3171 (1972).

[21] D. P. Spitzer, J. Phys. Chem. Solids **31**, 19 (1970).

[22] L. Fast, R. Ahuja, L. Nordström, J. M. Wills, B. Johansson, and O. Eriksson, Phys. Rev. Lett. **79**, 2301 (1997).

[23] M. J. Mehl, Phys. Rev. B **47**, 2493 (1993).

[24] F. Nitsche and B. Schumann, J. Low Temp. Phys. **39**, 119 (1980).

[25] R. E. Peterson and A. C. Anderson, J. Low Temp. Phys. **11**, 639 (1973).

[26] W. Kappus and O. Weis, J. Appl. Phys. **44**, 1947 (1973).

[27] P. Herth and O. Weis, Z. Angew. Phys. **29**, 101 (1970).

[28] M. J. P. Musgrave, *Crystal Acoustics* (American Institute of Physics, Melville, NY, 2003).

[29] W. G. Meyer and P. M. Parker, Acta Crystallogr. **14**, 725 (1961).

[30] W. M. Ewing, *Elastic Waves in Layered Media* (McGraw-Hill, New York, 1957).

[31] A Callaway-type expression $\kappa_{\text{lattice}} = C v \ell$ would suggest that the higher velocity longitudinal mode would be the largest contributor to thermal transport, but this is offset by the smaller region of phase space in which this sound velocity applies due to the intersection with optical branches (see Fig. 1) so that the ultimate apportionment of heat transfer among the various modes is not a trivial matter.

[32] T. Shiga, J. Shiomi, J. Ma, O. Delaire, T. Radzynski, A. Lusakowski, K. Esfarjani, and G. Chen, Phys. Rev. B **85**, 155203 (2012).

[33] G. A. Slack, Solid State Phys. **34**, 1 (1979).

[34] M. H. Grimsditch and A. K. Ramdas, Phys. Rev. B **11**, 3139 (1975).

[35] B. Houston, R. E. Strakna, and H. S. Belson, J. Appl. Phys. **39**, 3913 (1968).

[36] J. L. Feldman and D. J. Singh, Phys. Rev. B **53**, 6273 (1996).

[37] J. L. Mi, T. J. Zhu, X. B. Zhao, and J. Ma, J. Appl. Phys. **101**, 054314 (2007).

[38] M. Hichour, D. Rached, R. Khenata, M. Rabah, M. Merabet, A. H. Reshak. S. B. Omran, and R. Ahmed, J. Phys. Chem. Solids **73**, 975 (2012).

[39] A. Hamidani, B. Bennecer, and B. Boutarfa, Mater. Chem. Phys. **114**, 732 (2009).

[40] B. Kong, X.-R. Chen, J.-X. Yu, and C.-L. Cai, J. Alloys Compd. **509**, 2611 (2011).

[41] Y. Kawaharada, K. Kurosaki, H. Muta, M. Uno, and S. Yamanaka, J. Alloys Compd. **381**, 9 (2004).

[42] L. Manosa, A. Gonzalez-Comas, E. Obrado, A. Planes, V. A. Chernenko, V. V. Kokorin, and E. Cesari, Phys. Rev. B **55**, 11068 (1997).

[43] J. E. Graebner, S. Jin, G. W. Kammlott, J. A. Herb, and C. F. Gardinier, Appl. Phys. Lett. **60**, 1576 (1992).

[44] R. I. Cottam and G. A. Saunders, J. Phys. C **6**, 2105 (1973).

[45] S. P. R. Clark, P. Ahirwar, F. T. Jaeckel, C. P. Hains, A. R. Albrecht, T. J. Rotter, L. R. Dawson, G. Balakrishnan, P. E. Hopkins, L. M. Phinney, J. Hader, and J. V. Moloney, J. Vac. Sci. Technol. B **29**, 03C130 (2011).

[46] C. J. Glassbrenner and G. A. Slack, Phys. Rev. **134**, A1058 (1964).

[47] S. Uma, A. D. McConnell, M. Asheghi, K. Kurabayashi, and K. E. Goodson, Int. J. Thermophys. **22**, 605 (2001).

[48] H. J. McSkimmin and P. Andreatch, J. Appl. Phys. **35**, 2161 (1964).

[49] Note that the work of Ref. 43 in fact depicts a lattice thermal conductivity which varies significantly with grain size. For ease of comparison, we have chosen the value from the largest grain size.

[50] J. Androulakis, C.-H. Lin, H.-J. Kong, C. Uher, C.-I. Wu, T. Hogan, B. A. Cook, T. Caillat, K. Paraskevopoulos, and M. G. Kanatzidis, J. Am. Chem. Soc. **129**, 9780 (2007).

[51] K. Biswas, J. He, G. Wang, S.-H. Lo, C. Uher, V. P. Dravid, and M. G. Kanatzidis, Ener. Env. Sci. **4**, 4675 (2011).